

X-RAY EMISSION OF MARKARIAN 421: NEW CLUES FROM ITS SPECTRAL EVOLUTION. II. SPECTRAL ANALYSIS AND PHYSICAL CONSTRAINTS

G. FOSSATI

Center for Astrophysics and Space Sciences, University of California at San Diego, 9500 Gilman Drive, La Jolla, CA 92093-0424;
gfossati@ucsd.edu

A. CELOTTI, M. CHIABERGE, AND Y. H. ZHANG

International School for Advanced Studies, via Beirut 2-4, 34014 Trieste, Italy

L. CHIAPPETTI

Istituto di Fisica Cosmica G. Occhialini, via Bassini 15, 20133 Milano, Italy

G. GHISELLINI,¹ L. MARASCHI, AND F. TAVECCHIO

Osservatorio Astronomico di Brera, via Brera 28, 20121 Milano, Italy

E. PIAN

ITeSRE/CNR, via Gobetti 101, 40129 Bologna, Italy

AND

A. TREVES

Università dell'Insubria, via Lucini 3, 22100 Como, Italy

Received 2000 April 10; accepted 2000 April 21

ABSTRACT

Mrk 421 was repeatedly observed with *BeppoSAX* in 1997 and 1998. The source showed a very rich phenomenology with remarkable spectral variability. This is the second of two papers presenting the results of a thorough temporal and spectral analysis of all the data available to us, focusing in particular on the flare of April 1998, which was simultaneously observed also at TeV energies. The spectral analysis and correlations are presented in this paper, while the data reduction and timing analysis are the content of the companion paper. The spectral evolution during the flare has been followed over few ks intervals, allowing us to detect for the first time the peak of the synchrotron component shifting to higher energies during the rising phase and then receding. This spectral analysis nicely confirms the delay of the flare at the higher energies, which in Paper I we quantified as a hard lag of a few ks. Furthermore, at the highest energies, evidence is found of variations of the inverse Compton component. The spectral and temporal information obtained challenge the simplest models currently adopted for the (synchrotron) emission and, most important, provide clues on the particle acceleration process. A scenario accounting for all the observational constraints is discussed, where electrons are injected at progressively higher energies during the development of the flare and the achromatic decay is ascribed to the source light crossing time exceeding the particle cooling timescales.

Subject headings: BL Lacertae objects: general — BL Lacertae objects: individual (Markarian 421) — galaxies: active — X-rays: galaxies — X-rays: general

1. INTRODUCTION

Blazars are radio-loud AGNs characterized by strong variability, large and variable polarization, and high luminosity. Radio spectra smoothly join the infrared-optical-UV ones. These properties are successfully interpreted in terms of synchrotron radiation produced in relativistic jets and beamed into our direction because of plasma moving relativistically close to the line of sight (e.g., Urry & Padovani 1995). Many blazars are also strong and variable sources of GeV γ -rays, and in a few objects, the spectrum extends up to TeV energies. The hard X-ray to γ -ray radiation forms a separate spectral component, with the luminosity peak located in the MeV–TeV range. The emission up to X-rays is thought to be caused by synchrotron radiation from high-energy electrons in the jet, while it is likely that γ -rays derive from the same electrons via inverse Compton (IC) scattering of soft (IR-UV) photons—synchrotron or ambient soft photons (e.g., Sikora, Begelman, & Rees 1994; Ghisellini &

Madau 1996; Ghisellini et al. 1998). The contributions of these two mechanisms characterize the average blazar spectral energy distribution (SED), which typically shows two broad peaks in a νF_ν representation (e.g., Fossati et al. 1998a). The energies at which the peaks occur and their relative intensity provide a powerful diagnostic tool to investigate the properties of the emitting plasma, such as electron energies and magnetic field (e.g., Ghisellini et al. 1998). In X-ray bright BL Lac objects (HBL, from high-energy-peak BL Lacs, Padovani & Giommi 1995), the synchrotron maximum occurs in the soft-X-ray band.

Variability studies constitute the most effective means to constrain the emission mechanisms taking place in these sources as well as the geometry and modality of the energy dissipation.

The quality and amount of X-ray data on the brightest sources start to allow thorough temporal analysis as function of energy and the characterization of the spectral evolution with good temporal resolution.

Mrk 421 is the brightest HBL at X-ray and UV wavelengths and thus it is the best available target to study in detail the properties of the variability of the highest fre-

¹ Osservatorio Astronomico di Brera, via Bianchi 46, 22055 Merate (Lecco), Italy.

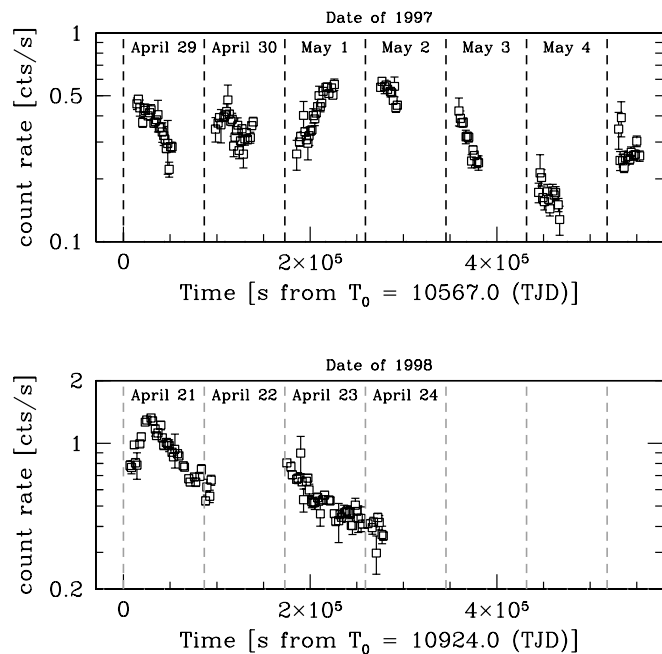


FIG. 1.—Light curves for the 1997 (top panel) and 1998 (bottom panel) campaigns, for the 4–6 keV MECS band. Binning time is 1500 s. Reference time TJD = 10567.0 corresponds to 1997 April 29:00:00 UT, and TJD = 10924.0 corresponds to 1998 April 21:00:00 UT.

quency portion of the synchrotron component, which traces the changes in the energy range of the electron distribution most critically affected by the details of the acceleration and cooling processes.

This paper is the second of two that present the uniform analysis of the X-ray variability and spectral properties from *BeppoSAX* observations of Mrk 421 performed in 1997 and 1998. In Paper I (Fossati et al. 2000), we presented the data reduction and the timing analysis of the data, which revealed a remarkably complex phenomenology. The study of the characteristics of the flux variability in different energy bands shows that significant spectral variability is accompanying the pronounced changes in brightness. In particular, a more detailed analysis of the remarkable flare observed in 1998 revealed that (1) the medium-energy X-rays lag the soft ones; (2) the postflare evolution is achromatic; and (3) the light curve is symmetric in the softest X-ray band, and it becomes increasingly asymmetric at higher energies, with the decay being progressively slower than the rise.

The general guidelines we followed for the data reduction and filtering are described in Paper I (in particular in § 2 and § 3.2). Here we will report only on details of the treatment of the data specific to the spectral fitting.

The paper is organized as follows. Sections 2 and 3 briefly summarize the basic information on *BeppoSAX* and the 1997 and 1998 observations. The results and discussion relative to the spectral analysis are the content of § 4 and § 5. In particular, the observed variability behavior strongly constrains any possible time-dependent particle acceleration prescription. We will therefore consider these results together with those of the temporal analysis, discuss which constraints are provided to current models, and present a possible scenario to interpret the complex spectral and temporal findings (§ 5.4). Finally, we draw our conclusions in § 6.

2. *BeppoSAX* OVERVIEW

For an exhaustive description of the Italian/Dutch *BeppoSAX* mission, we refer to Boella et al. (1997) and references therein. The results discussed in this paper are based on the data obtained with the Low- and Medium-Energy Concentrator Spectrometers (LECS and MECS) and the Phoswich Detector System (PDS). The LECS and MECS have imaging capabilities in the 0.1–10 keV and 1.3–10 keV energy band, respectively, with an energy resolution of 8% at 6 keV. The PDS covers the range 13–300 keV.

The present analysis is based on the SAXDAS linearized event files for the LECS and the MECS experiments, together with appropriate background event files, as produced at the *BeppoSAX* Science Data Center (“rev 0.2, 1.1 and 2.0”). The PDS data reduction was performed using the XAS software (Chiappetti & Dal Fiume 1997) according to the procedure described in Chiappetti et al. (1999).

3. OBSERVATIONS

Mrk 421 has been observed by *BeppoSAX* in the spring of 1997 and 1998. For reference, the *BeppoSAX* light curves for the 4–6 keV band are reported in Figure 1. Most of the forthcoming analysis is focused on the spectral variability observed during the flare of 1998 April 21, which is clearly visible in the bottom panel. The journal of observations is given in Table 1 of Paper I.

4. SPECTRAL ANALYSIS

To unveil the spectral variability during and after the flare, i.e., perform a time-resolved spectral analysis, we subdivided the whole data set in subintervals corresponding to single *BeppoSAX* orbits (42 for the 1997 data set, 16 on 1998 April 21, 19 on 1998 April 23) or a grouping of them sufficient to reach the same statistics (these are reported in Table 1, together with the median time [UTC] of each subinterval).

LECS and MECS spectra have been accumulated as described in Paper I. LECS data have been considered only in the range 0.12–3 keV because of calibration problems (a spurious hardening) at higher energies (M. Guainazzi, 1997, private communication).²

The nominal full-resolution spectra (i.e., channels 11–285 for 0.1–3 keV in the LECS and 36–220 for 1.6–10 keV in the MECS) then have been rebinned using the grouping templates available at *BeppoSAX*-SDC.³ The background has been evaluated from the blank fields provided by the

² A word of caution is necessary about localized features probably related with calibration problems yet to be solved (e.g., $E \sim 0.29$ keV, ~ 2 keV, in correspondence to the Carbon edge and the Gold features caused by the optics, respectively).

³ The energy resolution of the LECS and MECS detectors is lower than the energy spacing between instrumental calibrated channels (~ 10 eV for LECS and 45 eV for MECS). Therefore it is compelling to rebin the spectra, even in cases (like ours) where the statistics in each low-energy channel is good, in order to avoid to overweight (as $\chi_a^2 + \chi_b^2 > \chi_{a+b}^2$) information that is not truly independent. *BeppoSAX*-SDC templates are downloadable at <ftp://www.sdc.asi.it/pub/sax/cal/responses/grouping/>. Because of the very steep spectral shape, in order to maintain a good statistics in each new bin, we altered the templates for MECS above $\simeq 7$ keV, increasing the grouping of the original PI channels.

TABLE 1
LECS AND MECS CURVED MODEL SPECTRAL FIT: 1997 AND 1998^a

ORBITS	MEDIAN OBSERVING TIME (UTC)	SPECTRAL INDICES				E_B (keV)	E_{peak} (keV)	FLUXES ^b			χ^2_{ν} ^c
		0.5 keV	1 keV	5 keV	10 keV			0.2–1	2–10	0.1–10	
1997 April 29 to May 5											
1–3	1997/04/29:06:08	0.91 ^{+0.04} _{-0.04}	1.19 ^{+0.05} _{-0.04}	1.83 ^{+0.05} _{-0.05}	1.99 ^{+0.13} _{-0.10}	1.27 ^{+1.15} _{-0.62}	0.62 ^{+0.05} _{-0.05}	2.09	1.01	4.68	1.24
4–7	1997/04/29:11:43	1.00 ^{+0.03} _{-0.03}	1.28 ^{+0.04} _{-0.03}	1.93 ^{+0.05} _{-0.05}	2.09 ^{+0.11} _{-0.09}	1.34 ^{+0.96} _{-0.55}	0.49 ^{+0.04} _{-0.05}	1.89	0.75	4.07	1.03
8–10	1997/04/30:05:01	0.94 ^{+0.05} _{-0.06}	1.24 ^{+0.08} _{-0.08}	1.91 ^{+0.07} _{-0.06}	2.08 ^{+0.20} _{-0.13}	1.26 ^{+1.95} _{-0.75}	0.57 ^{+0.07} _{-0.08}	2.15	0.92	4.65	0.95
11–12	1997/04/30:08:37	1.01 ^{+0.04} _{-0.04}	1.24 ^{+0.05} _{-0.04}	1.91 ^{+0.07} _{-0.06}	2.11 ^{+0.21} _{-0.14}	1.99 ^{+2.65} _{-1.08}	0.48 ^{+0.07} _{-0.11}	1.96	0.83	4.29	0.94
13–15	1997/04/30:12:36	0.95 ^{+0.03} _{-0.03}	1.26 ^{+0.04} _{-0.04}	1.95 ^{+0.05} _{-0.05}	2.13 ^{+0.12} _{-0.09}	1.25 ^{+0.90} _{-0.53}	0.55 ^{+0.04} _{-0.04}	1.92	0.78	4.14	0.91
16–18	1997/05/01:05:08	1.03 ^{+0.05} _{-0.05}	1.35 ^{+0.07} _{-0.07}	1.84 ^{+0.07} _{-0.06}	1.94 ^{+0.13} _{-0.09}	0.57 ^{+0.91} _{-0.42}	0.46 ^{+0.05} _{-0.07}	1.99	0.76	4.20	1.14
19–20	1997/05/01:08:43	1.00 ^{+0.04} _{-0.04}	1.25 ^{+0.05} _{-0.05}	1.78 ^{+0.06} _{-0.05}	1.91 ^{+0.14} _{-0.10}	1.14 ^{+1.51} _{-0.66}	0.49 ^{+0.06} _{-0.08}	2.00	0.89	4.42	1.31
21–23	1997/05/01:12:39	0.92 ^{+0.03} _{-0.03}	1.20 ^{+0.04} _{-0.04}	1.86 ^{+0.04} _{-0.04}	2.04 ^{+0.11} _{-0.08}	1.44 ^{+0.98} _{-0.58}	0.61 ^{+0.04} _{-0.04}	2.60	1.22	5.79	1.21
24–25	1997/05/02:05:36	0.93 ^{+0.04} _{-0.04}	1.18 ^{+0.05} _{-0.04}	1.83 ^{+0.06} _{-0.05}	2.00 ^{+0.15} _{-0.11}	1.57 ^{+1.64} _{-0.85}	0.61 ^{+0.06} _{-0.07}	2.74	1.34	6.20	0.77
26–27	1997/05/02:08:35	0.93 ^{+0.05} _{-0.05}	1.24 ^{+0.06} _{-0.05}	1.88 ^{+0.06} _{-0.06}	2.03 ^{+0.15} _{-0.10}	1.08 ^{+1.27} _{-0.60}	0.58 ^{+0.06} _{-0.06}	2.56	1.12	6.20	1.03
28–30	1997/05/03:05:21	1.07 ^{+0.05} _{-0.05}	1.30 ^{+0.07} _{-0.05}	1.88 ^{+0.07} _{-0.07}	2.05 ^{+0.22} _{-0.14}	1.63 ^{+3.04} _{-1.05}	0.37 ^{+0.09} _{-0.19}	2.01	0.78	4.35	1.13
31–32	1997/05/03:08:38	1.05 ^{+0.06} _{-0.06}	1.28 ^{+0.06} _{-0.05}	2.13 ^{+0.09} _{-0.09}	2.49 ^{+0.39} _{-0.24}	3.50 ^{+6.97} _{-2.05}	0.39 ^{+0.12} _{-0.19}	1.65	0.62	3.63	0.79
33–34	1997/05/04:04:22	1.11 ^{+0.07} _{-0.07}	1.47 ^{+0.13} _{-0.10}	2.15 ^{+0.15} _{-0.12}	2.30 ^{+0.37} _{-0.20}	0.91 ^{+2.84} _{-0.75}	0.39 ^{+0.07} _{-0.20}	1.59	0.42	3.16	1.27
35–37	1997/05/04:07:55	1.21 ^{+0.05} _{-0.05}	1.49 ^{+0.08} _{-0.06}	2.14 ^{+0.10} _{-0.08}	2.31 ^{+0.25} _{-0.16}	1.38 ^{+2.42} _{-0.88}	0.23 ^{+0.11} _{-0.22}	1.60	0.40	3.25	0.92
38–40	1997/05/05:05:22	1.10 ^{+0.04} _{-0.04}	1.43 ^{+0.07} _{-0.06}	2.01 ^{+0.07} _{-0.07}	2.13 ^{+0.15} _{-0.11}	0.74 ^{+1.01} _{-0.47}	0.39 ^{+0.05} _{-0.09}	2.04	0.62	4.16	1.07
41–42	1997/05/05:08:46	1.10 ^{+0.06} _{-0.06}	1.35 ^{+0.08} _{-0.06}	1.98 ^{+0.10} _{-0.08}	2.15 ^{+0.29} _{-0.16}	1.61 ^{+3.73} _{-1.08}	0.33 ^{+0.10} _{-0.24}	1.88	0.65	4.00	0.62
1998 April 21											
1–2	1998/04/21:02:55	0.83 ^{+0.05} _{-0.06}	1.10 ^{+0.07} _{-0.06}	1.64 ^{+0.06} _{-0.06}	1.68 ^{+0.09} _{-0.07}	1.19 ^{+0.47} _{-0.34}	0.80 ^{+0.10} _{-0.08}	5.10	3.00	11.96	0.91
3	1998/04/21:05:07	0.87 ^{+0.05} _{-0.05}	1.02 ^{+0.04} _{-0.04}	1.65 ^{+0.08} _{-0.07}	1.74 ^{+0.15} _{-0.10}	1.82 ^{+0.74} _{-0.49}	0.92 ^{+0.12} _{-0.10}	5.34	3.46	13.08	0.97
4	1998/04/21:06:40	0.78 ^{+0.04} _{-0.04}	0.95 ^{+0.03} _{-0.03}	1.64 ^{+0.06} _{-0.06}	1.73 ^{+0.11} _{-0.09}	1.85 ^{+0.51} _{-0.38}	1.13 ^{+0.11} _{-0.10}	5.96	4.41	15.22	1.02
5	1998/04/21:08:19	0.81 ^{+0.04} _{-0.04}	0.96 ^{+0.03} _{-0.03}	1.58 ^{+0.05} _{-0.05}	1.66 ^{+0.08} _{-0.08}	1.82 ^{+0.64} _{-0.44}	1.09 ^{+0.12} _{-0.10}	5.77	4.22	14.63	0.86
6	1998/04/21:09:56	0.80 ^{+0.04} _{-0.04}	1.03 ^{+0.05} _{-0.04}	1.50 ^{+0.05} _{-0.05}	1.53 ^{+0.07} _{-0.06}	1.16 ^{+0.40} _{-0.30}	0.91 ^{+0.10} _{-0.09}	5.35	3.76	13.24	1.17
7	1998/04/21:11:32	0.79 ^{+0.04} _{-0.04}	1.00 ^{+0.05} _{-0.04}	1.53 ^{+0.06} _{-0.05}	1.57 ^{+0.08} _{-0.07}	1.36 ^{+0.46} _{-0.33}	0.98 ^{+0.11} _{-0.10}	5.05	3.62	12.64	0.85
8–9	1998/04/21:13:57	0.85 ^{+0.03} _{-0.03}	1.05 ^{+0.04} _{-0.03}	1.50 ^{+0.04} _{-0.04}	1.54 ^{+0.05} _{-0.05}	1.26 ^{+0.35} _{-0.27}	0.85 ^{+0.07} _{-0.06}	4.62	3.10	11.35	1.38
10–12	1998/04/21:17:57	0.87 ^{+0.02} _{-0.02}	1.05 ^{+0.03} _{-0.02}	1.54 ^{+0.04} _{-0.03}	1.58 ^{+0.05} _{-0.04}	1.40 ^{+0.30} _{-0.24}	0.85 ^{+0.06} _{-0.05}	3.99	2.63	9.76	0.89
13–16	1998/04/21:23:35	0.91 ^{+0.03} _{-0.03}	1.06 ^{+0.03} _{-0.02}	1.61 ^{+0.05} _{-0.05}	1.67 ^{+0.08} _{-0.07}	1.67 ^{+0.48} _{-0.36}	0.79 ^{+0.07} _{-0.07}	3.61	2.23	8.73	0.99
1998 April 23											
1–5	1998/04/23:03:49	0.93 ^{+0.02} _{-0.03}	1.10 ^{+0.03} _{-0.02}	1.67 ^{+0.04} _{-0.04}	1.74 ^{+0.07} _{-0.05}	1.59 ^{+0.37} _{-0.29}	0.71 ^{+0.05} _{-0.05}	4.15	2.32	9.74	1.11
6–11	1998/04/23:12:31	0.95 ^{+0.02} _{-0.02}	1.17 ^{+0.02} _{-0.02}	1.78 ^{+0.03} _{-0.03}	1.84 ^{+0.05} _{-0.04}	1.47 ^{+0.21} _{-0.18}	0.60 ^{+0.03} _{-0.04}	3.73	1.78	8.42	1.27
12–19	1998/04/23:23:39	1.03 ^{+0.02} _{-0.02}	1.19 ^{+0.02} _{-0.02}	1.79 ^{+0.04} _{-0.04}	1.85 ^{+0.06} _{-0.05}	1.68 ^{+0.32} _{-0.26}	0.38 ^{+0.09} _{-0.23}	3.25	1.47	7.30	1.16

^a Since there are always three varying parameters—either two α and E_B or one α , one E and E_B —all the quoted errors are for 1σ for three parameters (i.e., $\Delta\chi^2 = 3.53$), a quite conservative choice.

^b Unabsorbed fluxes in units of 10^{-10} ergs cm^{-2} s^{-1} , in the reported energy band, the boundaries of which are expressed in keV.

^c The degrees of freedom are 57 for all cases.

BeppoSAX-SDC,⁴ using an extraction region similar in size and position to the source extraction region. The 1998 November release of public calibration files, matrices, and effective areas was used.

For the PDS spectra, we applied the improved screening, implementing the temperature and energy dependence of the pulse rise time (so-called PSA correction method).

Owing to a slight mismatch in the cross-calibration among the different detectors, it has been necessary to include in the fitting models multiplicative factors of the normalization (LECS/MECS and PDS/MECS ratios). The correct absolute flux normalization is provided by the MECS (the agreement between MECS units is within the 2%–3% limit of the systematics). The expected value of these constant factors is now well known and does not constitute a major/additional source of uncertainty. According to Fiore, Guainazzi, & Grandi (1999), the acceptable range for LECS/MECS is 0.7–1.0, with some depen-

dence on the source position in the detectors, while the PDS/MECS ratio can be constrained between 0.77 and 0.95. The latter parameter is indeed crucial in sources like Mrk 421 where there is a significant possibility that a different component arises in the PDS range, the recognition of which critically depends on the capability/sensitivity to reject the hypothesis that the PDS counts can be accounted for by the extrapolation of the LECS-MECS spectrum (see § 4.3.3).

4.1. Single and Broken Power Laws

We do not discuss in detail any power-law spectral models. For each LECS + MECS spectrum, we fit the data with the single and the broken power-law models,⁵ both with free and fixed⁶ absorbing column density.

⁵ In Appendix C, Table 6 reports the best-fit values for the relevant parameters for the broken power-law model.

⁶ In the direction of Mrk 421, the Galactic equivalent absorbing column is $N_H = (1.61 \pm 0.1) \times 10^{20}$ cm^{-2} (Lockman & Savage 1995), with the estimated uncertainty for high Galactic latitudes.

⁴ Blank fields event files were accumulated on five different pointings of empty fields and are available at the anonymous ftp: ftp://www.sdc.asi.it/pub/sax/cal/bgd/.

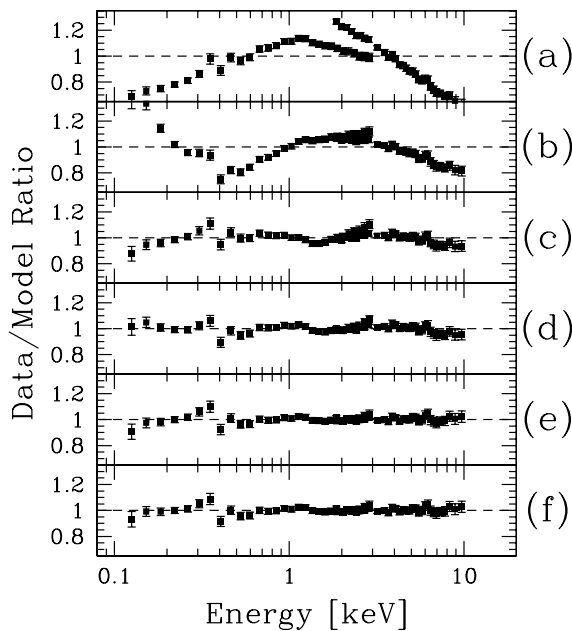


FIG. 2.—Data/Model ratios for different spectral models applied to the 1998 data. *Top to bottom*: single power law, with (a) Galactic and (b) free absorbing column; broken power law, with (c) Galactic and (d) free absorbing column; curved model, with (e) Galactic and (f) free absorbing column. Corresponding values of χ^2 are reported in Table 2.

Here we just show that they are an inadequate description of the downward curved spectra.⁷ To illustrate the discrepancy, we took the data/model ratio for the best-fit continuum model for each of the individual LECS + MECS spectra (16 for 1997; 12 for 1998), and we summed all of them, propagating the errors accordingly. The results are shown in Figure 2 for the 1998 data only, while in Table 2 we report the total χ^2 value for each trial model, together with the (simple) average value of N_{H} for fits with free absorption.

Neither the single nor the broken power laws provide an adequate representation of the data, not even when the value of the absorbing column density is left free to vary⁸—a common workaround used when the spectrum

⁷ In Fossati et al. (1998b) we presented a preliminary analysis of 1997 data, where LECS and MECS spectra have been fit with a variety of combinations of single and broken power-law models to better describe the spectral curvature. We refer the interested reader to that work.

⁸ Although the plot shown in Fig. 2d could appear as a good fit, the significance of the small deviations above a few keV is indeed high, yielding an unsatisfactory fit.

shows either a soft excess or a marked steepening toward higher energies (e.g., Takahashi et al. 1996).

Indeed, the description of the curvature by means of soft X-ray absorption is not only unphysical, but it hinders the possibility of extracting all the information from the data by leaving as meaningful parameter only the higher energy spectral index and accounting for all the other effects by N_{H} . Furthermore, this yields spectral indices that are only rough estimates, as it is clear that the best-fit single power law does not describe the observed data in any (even narrow) energy range (see Figs. 2a, 2b). Finally, in the case of Mrk 421 there is no reason to postulate any intrinsic absorbing component responsible for the observed spectral curvature (see also § 4.3.2).

4.2. The Curved Model

Motivated by the failure of the simplest power-law models, we developed a spectral model that is intrinsically curved,⁹ the aim of which is extracting all the information contained in the data and, in particular, estimate the position of the peak of the synchrotron component—one of the crucial quantities in blazars modeling.

A spectral model providing an improved description of the continuum shape also allows a more sensitive study of discrete spectral features such as absorption edges, the presence of which has been long searched in the soft X-ray blazars spectra (e.g., Canizares & Kruper 1984; Sambruna et al. 1997; Sambruna & Mushotzky 1998).

We started from the following general description of a continuously curved shape (see e.g., Inoue & Takahara 1996; Tavecchio, Maraschi, & Ghisellini 1998):

$$F(E) = KE^{-\alpha_{-\infty}} \left[1 + \left(\frac{E}{E_B} \right)^f \right]^{(\alpha_{-\infty} - \alpha_{+\infty})/f}, \quad (1)$$

where $\alpha_{-\infty}$ and $\alpha_{+\infty}$ are the asymptotic values of spectral indices for $E \ll E_B$ and $E \gg E_B$, respectively, while E_B and f determine the scale length of the curvature.

We reexpressed this function in terms of the spectral indices at finite values of E , which characterize the local shape of the spectrum, instead of the asymptotic ones, which do not have any direct reference to the observed portion of the spectrum.

The spectral model is then expressed in a form such that the available parameters are $(E_1, \alpha_1, E_2, \alpha_2, E_B, f)$ instead of $(\alpha_{-\infty}, \alpha_{+\infty}, E_B, f)$ (for more details see Appendix B). As we have two extra parameters, for a meaningful use of this spectral description we have to fix one for each of the pairs

⁹ In Appendix A, we discuss an important caveat concerning the definition of curved models.

TABLE 2
SUMMARY OF POWER-LAW MODELS RESULTS

MODEL	1997				1998			
	N_{H}^a	χ^2	χ^2_{ν}	dof	N_{H}^a	χ^2	χ^2_{ν}	dof
Single power law	Galactic	11903.1	12.609	944	Galactic	11245.0	15.883	708
Single power law	3.78 ± 0.18	3012.7	3.246	928	3.22 ± 0.14	3413.2	4.905	696
Broken power law	Galactic	1162.6	1.275	912	Galactic	997.6	1.458	684
Broken power law	2.23 ± 0.46	1083.2	1.209	896	2.05 ± 0.19	866.6	1.289	672
Curved	Galactic	935.7	1.026	912	Galactic	721.1	1.054	684
Curved	1.73 ± 0.12	917.8	1.024	896	1.70 ± 0.12	705.2	1.049	672

^a Absorbing column units are 10^{20} cm^{-2} .

(E_1, α_1) and (E_2, α_2). Eventually, this degeneracy turns out to be a powerful property of this model because it allows us to derive the spectral index at selected energies (setting E_i at the preferred values) or, even more interestingly, to estimate the energy at which a certain spectral index is obtained (setting α_i at the desired value). The most relevant example of this latter possibility is the determination of the position of the peak (as seen in νF_ν representation) of the synchrotron component E_{peak} —if it falls within the observed energy band—and the estimate of the associated error. This can be obtained by setting one spectral index, i.e., $\alpha_1 = 1$ and leaving the corresponding energy E_1 free to vary in the fit. The best-fit value of $E(\alpha = 1)$ gives E_{peak} .

4.3. Results

Most of the spectral analysis with the curved model has been performed by keeping the absorbing column fixed to the Galactic value to remove the degeneracy between the effects of a variable absorption and intrinsic spectral curvature. We will briefly comment on the fits with a variable absorbing column in the next section.

To determine the values for the really interesting parameters, we tried a set of values for the parameter f ranging from 0.5 to 3 (with a step of 0.5). All other parameters were left free to vary during these step-fits. We then selected the value of f yielding the minimum total χ^2 . The best-fit value for 1997 is $f = 1$, while for 1998 $f = 2$, as expected from the stronger curvature of the spectra. In Table 1, we report the spectral parameters, together with the 0.2–1, 2–10, and 0.1–10 keV fluxes (dereddened) and χ^2 values, for each of the time-sliced spectra. The global Data/Model ratio is shown in Figure 2e, and the total χ^2 is reported in Table 2. The curved model is strongly preferred also from the purely statistical standpoint: in fact, the model with Galactic N_{H} has a significantly better χ^2 than the broken power law with free N_{H} , although it has one less adjustable parameter (i.e., one more degree of freedom).

Each spectrum has been fitted a few times in order to derive spectral indices at several energies (0.5, 1, 5, 10 keV) and also E_{peak} . For consistency, we checked each time that not only the value of the χ^2 remained the same but also that all the other untouched parameters took the same value and confidence intervals. The fits are indeed very robust in this sense.

The main new result is that we were able to *determine the energy of the peak of the synchrotron component* and to assign an error to it. This has been possible with reasonable accuracy for both 1997 and 1998 spectra, with a couple of cases yielding only an upper limit for the peak energy.¹⁰

An example of the remarkable spectral evolution during the 1998 flare is shown by the deconvolved spectra in Figure 3, which also illustrates the strong convexity of the spectrum and the well-defined peak.

In 1997, the source was in a lower brightness state, with an average X-ray spectrum softer (at all energies $\Delta\alpha_{9.7-9.8} \simeq 0.4$) and a peak energy 0.5 keV lower.

More globally, the analysis shows that there is a clear relation between the flux variability and the spectral parameters, both in 1998 and, albeit less strikingly, in 1997. Particularly important is the correlation between changes in the

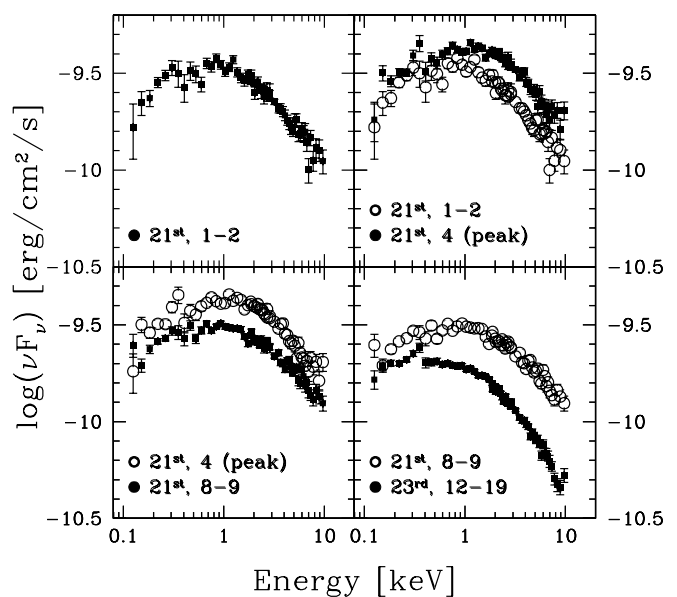


FIG. 3.—Inferred *BeppoSAX* νF_ν spectra of Mrk 421 in 1998. Plotted spectra correspond to the orbit groupings 1 + 2, 4, 8 + 9 of April 21, and 12–19 of April 23 (see Table 1). For comparison, we also plotted in light gray color the spectrum of the previous box.

brightness (even the small ones) and shifts of the peak position, as the latter carries direct information on the source’s physical properties. In Figures 4a and 4b, α at 5 keV and E_{peak} for 1997 and 1998 are plotted versus the 0.1–10 keV flux. The source reveals a coherent spectral behavior between 1997 and 1998 and through a large flux variability (a factor 5 in the 0.1–10 keV band). Both the peak energies and the spectral indices show a tight relation with flux, the latter being described by $E_{\text{peak}} \propto F^\epsilon$, with $\epsilon = 0.55 \pm 0.05$.

4.3.1. Hard Lag in 1998 Spectra

One further important finding of the time-resolved spectral study is the signature of the hard lag, which strengthens what was already inferred from the timing analysis (see Paper I). In fact, the local spectral slope at different energies indicates that the flare starts in soft X-rays and then extends to higher energies.

A blow-up of the 1998 flare interval is shown in Figure 5: spectral indices at 1 and 5 keV, and E_{peak} are plotted versus time in the left-hand plots and versus flux in the right-hand ones. The synchrotron peak shifts toward higher energies during the rise and then decreases as soon as the flare is over. The spectral index at 1 keV reflects exactly the same behavior, as expected being computed at the energy around which the peak is moving (and, in fact, it moves in a narrow range around $\alpha = 1$). On the contrary, the spectral shape at 5 keV does not vary until a few ks after the peak, and only then—while the flux is decaying and the peak is already receding—is there a response with a significant hardening of the spectrum. The right-side diagrams illustrate this behavior directly in terms of flux: the evolution of the peak energy and the 1 keV spectral shape follow closely that of the flare, while at 5 keV the spectrum does not change shape until after the peak.

Thus, the spectral evolution at higher energies develops during the decay phase of the flare, tracing a loop in the α versus Flux diagram, with a significant hardening of the

¹⁰ These are the cases “35–37” and “41–42” of 1997. Actually, the formal fitting yields a confidence interval but with the lower extreme falling outside of the observed energy range.

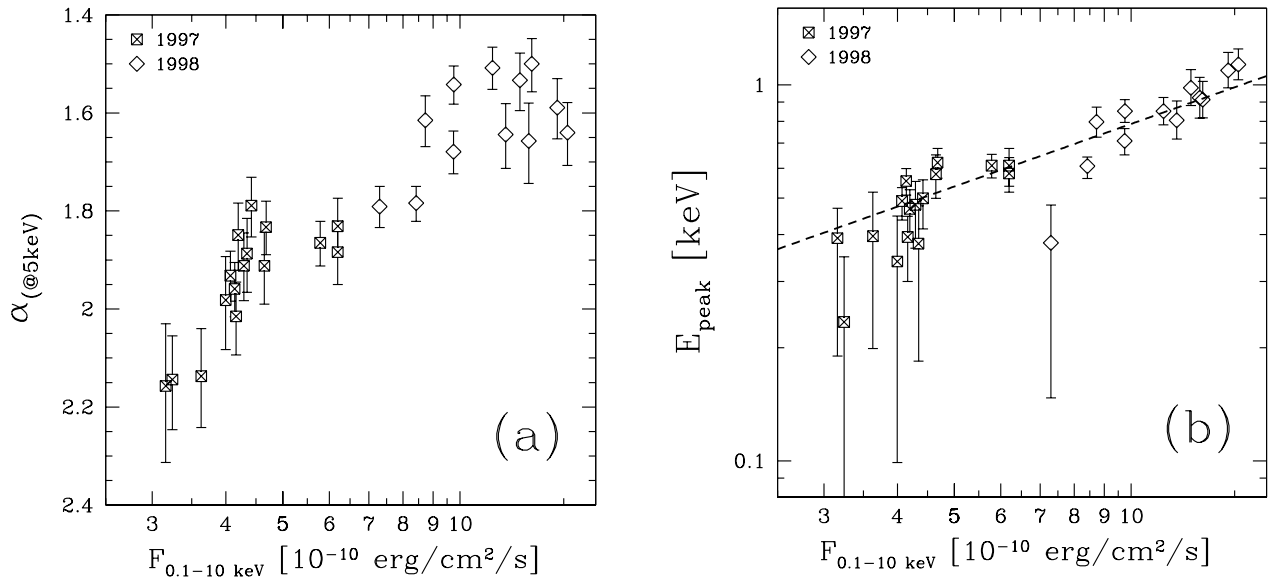


FIG. 4.—(a) Spectral index at 5 keV and (b) synchrotron peak energy plotted vs. the deabsorbed 0.1–10 keV flux, both for 1997 and 1998 data sets. The dashed line across diagram (b) represents the best-fitting power law, with a slope $\epsilon = 0.55$.

spectrum. Because of the presence of the hard lag, the loop is traced in the *opposite* way with respect to evolution that is commonly observed during flares in HBL, that is, a spectral hardening during the rise of the outburst followed by a softening during the decay (see, however, Sembay et al. 1993; Catanese & Sambruna 2000).

This behavior—usually accompanied by a soft lag—produces a clockwise loop in α versus Flux.

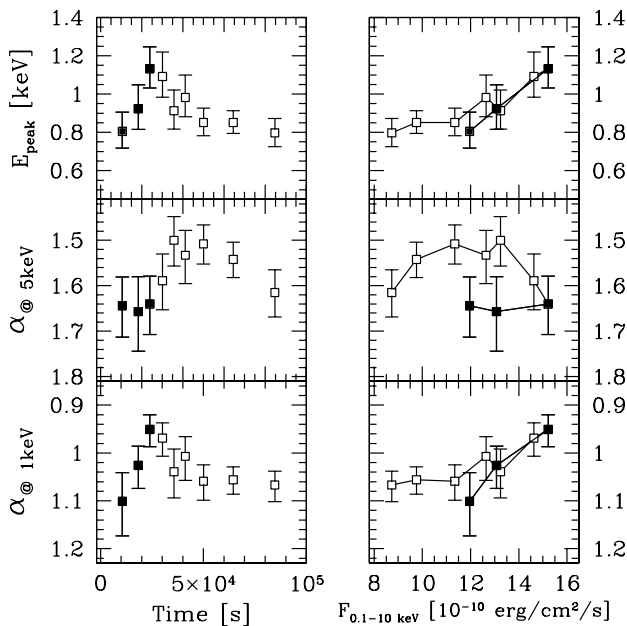


FIG. 5.—*Top to bottom*: Energy of the peak of the synchrotron component, and photon spectral indices at 5 and at 1 keV vs. time (*left column*) and deabsorbed 0.1–10 keV flux (*right column*). Solid black symbols represent the behavior before the top of the flare, while empty dots represent the spectral evolution during the decay. Data points are connected to show the time sequence. A shift of the synchrotron peak and a delay in the response of the spectrum at 5 keV can be seen clearly.

4.3.2. Absorption Features: N_{H} and Edges

We also fitted the 1997 and 1998 spectra with the curved spectral model leaving the N_{H} free to vary. The only constraint that we imposed is on the exponent f , which is set at the best-fit values of $f = 1$ and $f = 2$ for 1997 and 1998, respectively. The improvement of the global fit¹¹ is not statistically significant. The average best-fit absorbing column is indeed very close to and consistent with the Galactic one, leading us to conclude that there is no requirement whatsoever for an additional absorbing column to model the data.

We searched for the presence of absorption edges at low energies ($E \lesssim 1$ keV) both in 1997 and 1998 data. We added to the curved continuum an absorption edge, with a first-guess fit at $E \simeq 0.4$ – 0.5 keV, as even in the case of the best curved model with free N_{H} there are residues around this energy (see Fig. 2f). The most delicate issue is the calibration problem related with the instrumental carbon absorption edge at 0.29 keV. Even the smallest uncertainties ($\sim 1\%$ – 2%) in the knowledge of the instrument response around this energy can induce significant spurious features, typically at slightly higher energy (see Fossati & Haardt 1997).

There is not convincing evidence for discrete absorption features. In 5/28 cases the fit routine has not found an edge, while there are indeed a few spectra (8/28) in which the fit definitely put the edge at 0.27–0.30 keV to account for systematic deviation caused by calibration uncertainties. There are then 15/28 cases where the edge energy is around 0.4–0.6 keV, but, again, only in a handful of cases is the best-fit energy E_{edge} significantly different from 0.29 keV.

Summarizing, there are only three individual spectra (of 28) for which the inclusion of the edge is formally statistically significant ($>95\%$), according to the F-test. These

¹¹ $\Delta\chi^2 = 17.9$ for 16 additional dof for 1997 and $\Delta\chi^2 = 15.9$ for 12 additional dof for 1998, corresponding to an average $\Delta\chi^2 \simeq 1.2$ per spectrum for a change in dof from 57 to 56.

three cases do not stand out in the sample for any other property, such as brightness or curvature of the continuum. Best-fit energies and optical depths are typically $E_{\text{edge}} \simeq 500_{-100}^{+50}$ eV, and $\tau \simeq 0.4_{-0.2}^{+0.3-0.6}$. However, considering that the sample comprises 28 spectra, with the significance threshold set at 95%, three positive detections cannot be regarded as a compelling evidence for the presence of absorption edges.

4.3.3. PDS Data

Covering the range above $\simeq 12$ keV, the PDS instrument could detect the IC component, which might start to dominate the emission in this band. It has always proven to be very difficult to detect/constrain this component, although it is expected to have a very hard spectrum, which should make it easier to disentangle from the very steep tail of the synchrotron component. There are a few objects, the so-called intermediate BL Lac objects, in which the crossover between synchrotron and IC occurs in the 0.1–10 keV band, for which it has then been possible to clearly detect the hard IC power law, with typical $\alpha \simeq 0.3$ –0.7 (e.g., Tagliaferri et al. 2000 for ON 231; Giommi et al. 1999 for S5 0716+714; Sambruna et al. 1999 for BL Lac). The good sensitivity of the PDS yielded a convincing evidence of IC emission in the case of PKS 2155–304 (Giommi et al. 1998). The preliminary analysis of the Mrk 421 1997 data (Fossati et al. 1998b) suggested the presence of a hard component. We therefore focused on the search for the IC component for both of 1997 and 1998 PDS data sets.

For 1998, when the source was brighter, we accumulated PDS spectra according to the same partition of the light curves used for the 0.1–10 keV data. In most of the individual spectra there is a significant ($\geq 3\sigma$) detection only up to 40 keV. The light curve for the 12–26 keV band is shown in Figure 3 of Paper I.

We then restricted the analysis to only one spectrum for 1997, integrating over the whole campaign, and two for 1998, one for April 21, and one for April 23. The integration times are 54.8, 21.1, and 25.2 ks, respectively (see Paper I). We grouped the data in six spectral channels with boundaries at 12, 18, 27, 40, 60, 90 and 130 keV.

In the 1997 spectrum there is a positive detection up to 90 keV. For April 21—corresponding to the synchrotron flare—there is a strong signal up to 60 keV, while, surprisingly, in the April 23 spectrum there is a $\gtrsim 3\sigma$ detection in each individual bin up to 130 keV. From 12 to 40 keV, the April 21 count rates are significantly higher than those of April 23, but while the former continue to steeply decrease with increasing energy, the latter flatten above 40 keV, with a crossover in the 40–60 keV bin. As the integra-

tion times for these two spectra are similar (and in fact statistical uncertainties on the count rate are of the same order), this cannot account for this difference.¹²

The results of single power law fits are reported in Table 3. Clearly the April 23 spectrum is significantly harder. Moreover, the spectral indices for the first two cases are consistent with those derived from the LECS and MECS data sets and the general picture of a continuously steepening spectrum, while this does not hold for the third case.

While this is already interesting, there is one additional, somehow unexpected, finding: apparently the April 23 harder spectrum cannot be simply interpreted as the detection of the IC component when the synchrotron tail recedes. In fact, a hard power law at this flux level—if present—would have been detected on April 21 also, while the count rates in the higher energy bins for April 21 set a tight upper limit. This behavior might be ascribed to either a different independent origin or a delayed response of the IC component with respect to the synchrotron one (indeed some evidence of a possible delayed decay of the PDS with respect to the MECS emission can be seen in the light curves).

Finally, we tried to quantify the presence of the IC power law in the three data sets by fitting MECS and PDS data together. We proceeded in the following way.

1. We accumulated LECS and MECS spectra over the same intervals of the PDS ones, i.e., one cumulative spectrum for each day of 1998, and one for the whole 1997.
2. We fit the LECS + MECS spectra in order to constrain the average synchrotron spectrum.
3. We then fixed all the parameters of the curved model to the LECS + MECS best-fit values and added to the model a hard power-law component¹³ with a fixed spectral index (we tried the values $\alpha_{\text{IC}} = 0.4, 0.5, 0.6, 0.7$). We also added an exponential cut-off to the synchrotron component, setting its two parameters, i.e., cut-off and e -folding energies, to 10 and 40 times the best-fit value of E_{peak} .

¹² Also, we are not aware of any intraobservation “background fluctuations” to be taken into account in the standard PDS data reduction (which has been performed by carefully following the prescriptions given by the instrument team—for all the details, refer to Chiappetti et al. 1999) nor of any long-term “background fluctuations” that could be responsible for the observed variation. No such thing was reported either by the PDS instrument team or by the *BeppoSAX* Science Data Center.

¹³ We used the “pegpwr1w” (power law with pegged normalization) model of XSPEC that provides a robust measure of the normalization. In fact, this is defined over a selectable energy band instead of the monochromatic value at 1 keV that can be strongly correlated with other parameters if 1 keV does not fall close to the logarithmic median of the band spanned by the data.

TABLE 3
PDS SINGLE POWER-LAW FITS: 1997 AND 1998

DATA SET	BAND (keV)	EXPOSURE (ks)	COUNT RATES		α^a	$F_{1 \text{ keV}}$ (μJy)	χ^2	dof
			12–40 keV (cts s ⁻¹)	40–90 keV (cts s ⁻¹)				
1997	12–90	54.8	0.177 ± 0.021	0.045 ± 0.019	2.17 ^{+0.48} _{-0.41}	1.52	2.96	3
1998 April 21.....	12–90	21.1	0.698 ± 0.028	0.039 ± 0.023	2.23 ^{+0.14} _{-0.13}	5.76	1.76	3
1998 April 23.....	12–90	25.2	0.293 ± 0.025	0.081 ± 0.021	1.35 ^{+0.26} _{-0.24}	1.35	6.95	4
	12–130	1.54 ^{+0.28} _{-0.25}	1.54	2.95	3

^a Errors are for 1 σ for one parameter (i.e., $\Delta\chi^2 = 1.0$).

4. We used this partially constrained model to fit the MECS (above $E \geq 5$ keV) and PDS spectra. The two 1998 data sets have been fit jointly with PDS/MECS inter-calibration factor free to vary, but set to be the same for both, and of course independent normalization.

The results are reported in Table 4 for the $\alpha_{\text{IC}} = 0.5$ case (the values relative to the other α_{IC} are not significantly different). The best-fit PDS/MECS normalization ratio is 0.88.

There seems to be a significant change in the flux level of the expected IC component between 1998 April 21 and 23. The best-fit value for the normalization for the first day is zero, while for the second day a nonzero IC flux is definitely required. To test the likelihood of the apparent variation, we fit the data constraining the normalization to be the same for the two data sets (third case in Table 4), and the F-test probability to obtain by chance the observed change in χ^2 is ~ 0.01 ($\Delta\chi^2 = 6.08$, degrees of freedom [dof] from 30 to 31).

The basic result for 1997 is that the IC component is definitely detected. Its brightness level is comparable with the average of 1998, while the synchrotron component shows a significant variation.

It should be noted that the synchrotron fluxes reported in Table 4 are not the best reference because at those energies, well above the synchrotron peak, the spectrum is very steep and even the smallest shift of the peak energy translates in a big change in the flux. Nevertheless, even when considering the energy range 0.1–10 keV, which includes the synchrotron peak, the variation between 1997 and 1998 is of the order of a factor of 2–3 (e.g., Fig. 5). The sampling of the 1997 light curve is not good enough to enable us to investigate any possible variation of the PDS spectrum with the source brightness.

5. DISCUSSION

Before focusing on the modeling of the temporal and spectral behavior illustrated in this paper and in Paper I, let us consider a few issues we regard as being of particular relevance for the interpretation of the origin of blazar variability.

5.1. Spectral Variability, Synchrotron Peak, and IC Component

Soft and hard X-ray bands show a different behavior. This might be attributed to the contribution from both the synchrotron and inverse Compton components at these energies. As electrons emitting X-rays through the two processes would have different energies, the two components

are not expected to vary on the same timescales and in phase. Indeed, on one hand the constraints provided by the analysis of the PDS data suggest that the synchrotron component constitutes the dominant contribution to the flux in the 12–26 keV band on 1998 April 21 (during the flare) with a light curve somewhat different from that of the softer synchrotron X-rays. On the other hand, the evidence supporting the possibility of a substantial variation in the IC component during the 1998 observations is extremely interesting. We can rule out the possibility that the flux level of the hard component is approximately constant between the two observations of 1998 (with a 99% confidence) and, thus, that its detectability only depends on the brightness level of the tail of the synchrotron emission.

5.2. The Flaring Plus Steady Components Hypothesis

A further interesting issue raised in Paper I in connection with the temporal analysis is the presence and role of quasi-stationary emission. Our results support the view that the short-timescale, large-amplitude variability events could be attributed to the development of new individual flaring components, giving rise to a spectrum outshining a more slowly variable contribution.

Indeed there is growing evidence that the overall blazar emission comprises a component that is (possibly) changing only on long timescales and that does not take part in the flare events (see, for instance, Mrk 501, Pian et al. 1998 and 1999, for the case of the UV variability of 3C 279).

The deconvolution of the SED into different contributions would allow the study of the evolution of the flaring component, thus possibly clarifying the nature of the dissipation events occurring in relativistic jets—in particular, the particle acceleration mechanism—and the modality and temporal characteristics of the initial release of plasma and energy through these collimated structures.

The deconvolution, however, is still difficult to achieve with the available temporal and spectral information. In Paper I we discussed the results of our attempt to measure directly the relative contributions of what we identify as steady and flaring components (parameter \mathcal{R}) from the characteristics of the flare decay. The result is very interesting, although it does not provide a useful handle on the evolving spectral properties of the flare itself. A more feasible approach is to assume specific forms of the flare evolution and test them against the data. One of the simplest working hypotheses is to assume that the flare evolution can be reproduced by the time-dependent flux and energy shifts of a peaked spectral component with fixed spectral shape (e.g., Krawczynski et al. 2000). In this context, it is

TABLE 4
HIGH-ENERGY COMPONENT CONSTRAINTS FROM MECS + PDS SPECTRAL FITS

DATA SET	HIGH-ENERGY COMPONENT FLUX ^{a,b}		SYNCHROTRON FLUX ^{a,c}		χ^2	dof
	12–40 keV	40–100 keV	12–40 keV	40–100 keV		
1997	$11.0^{+2.1}_{-2.6}$	$12.8^{+3.7}_{-2.1}$	7.8	0.2	17.92	15
1998 April 21	$<13.0^d$	$<14.9^d$	78.4	8.6	28.71	30
1998 April 23	$13.6^{+3.3}_{-3.1}$	$15.8^{+3.8}_{-3.6}$	24.0	1.2
1998 April 21 + 23	$10.1^{+3.1}_{-2.9}$	$11.8^{+3.5}_{-3.4}$	78.4 / 24.0	8.6 / 1.2	34.79	31

^a Fluxes are in units of 10^{-12} ergs cm^{-2} s^{-1} . Errors are for 1σ for one parameter (i.e., $\Delta\chi^2 = 1.0$).

^b Flux computed by the best-fit model in the hard power law.

^c Flux computed by the best-fit model in the curved model component.

^d 90% upper limit.

relevant to remind ourselves that the maximum of the synchrotron emission corresponds to the energy at which most of the energy in particles is located. Its value and temporal behavior thus trace the evolution of the bulk of the energy deposition into particles by the dissipation mechanism.

It is therefore possible that the variability characteristics (both temporal and spectral) might chiefly depend on the (particles/photons) energy *relative* to the synchrotron peak. In particular, the results on T_{short} (Paper I) can be either related to the dominance of the light crossing time over the cooling timescales or, alternatively, to the different position of the sampled energies with respect to the synchrotron peak as, above the peak, the timescales are shorter. In any case, the fact that timescales are similar at the different energies possibly indicates the evolution of a (observed) fixed-shape flaring component.

5.3. Sign of the Lag

One of the main new results of the temporal analysis presented in Paper I is the significant detection of a hard lag, opposite of the behavior commonly detected in HBL. Interestingly, a recent study by Zhang et al. (1999) on the source PKS 2155-304 has shown the presence of an apparent inverse trend between the source brightness level and the duration of the (soft) lag. And, intriguingly, the 1998 flare represents the brightest state ever observed from Mrk 421, thus possibly suggesting that an extrapolation of the above phenomenological trend might even account for a hard lag. This possibility is currently under study (Y. H. Zhang et al., in preparation).

Again, the relative contribution of two components might be responsible for this trend. During the most intense events, the flaring component would completely dominate over the quasi-stationary one, progressively shifting to higher energies (hard lag) while in weaker flares the varying component would exceed the steady one only at energies higher than the peak, where the spectrum steepens, producing an observed soft lag behavior.

However, one should also consider that in different brightness states the different observed energies correspond to different positions with respect to E_{peak} (e.g., in comparing the 1997 and 1998 data sets we showed that its value was typically a factor 2 different), requiring a more subtle analysis before deriving inferences on the lag-brightness relationship.

5.4. Physical Interpretation: The Signature of Particle Acceleration

Let us now focus on the interpretation of the two main and robust results of this work, namely, the hard lag and the evolution of the synchrotron peak.

The occurrence of the peak at different times for different energies is most likely related to the particle acceleration/heating process. Although models to reproduce the temporal evolution of a spectral distribution have been developed (e.g., Chiaberge & Ghisellini 1999; Georganopoulos & Marscher 1998; Kirk, Rieger, & Mastichiadis 1998), they mostly do not consider the role of particle acceleration (see, however, Kirk et al. 1998).

To account for the above results, we thus introduced a (parametric) acceleration term in the particle kinetic equation within the time-dependent model studied by Chiaberge & Ghisellini (1999). In particular, this model takes into account the cooling and escape in the evolution of the particle distribution and the role of delays in the received photons caused by the light crossing time of different parts of the emitting region.

The model includes the presence of a quiescent spectrum, which is assumed to be represented by and thus fitted to the broadband spectral distribution observed in 1994 (Macomb et al. 1995). To this a flaring component is added, and this is constrained by the observed spectral and temporal evolution (the parameters for both the stationary and variable spectra are reported in Table 5). The values of the model parameters are very close to those derived in Maraschi et al. (1999) in a somewhat independent way, i.e., trying only to fulfill the constraints provided by the X-ray and TeV spectra, that is simultaneous but averaged over the whole flare. On this basis, it is very likely that the model discussed here satisfies the TeV constraints, which are however not taken directly into account (the computation of the TeV light curve in this complex model would require treating the nonlocality of the IC process, which is beyond the scope of this paper).

Clearly a parametric prescription does not reproduce a priori a specific acceleration process, but we rather tried to constrain its form from the observed evolution. The main constraints on the form of the acceleration term are as follows.

1. Particles have to be injected at progressively higher energies on the flare-rise timescale to produce the hard lag.
2. Globally, the range of energies over which the injection occurs has to be narrow to give rise to a peaked spectral component.
3. A quasi-monochromatic injection function is needed for the flux at the highest energies to reach its maximum *after* that at lower ones (as opposed to, e.g., a power law with increasing maximum electron Lorentz factor).
4. The emission in the LECS band from the particles that have been accelerated to the highest energies (i.e., those radiating initially in the MECS band) should not exceed

TABLE 5
MODEL PARAMETERS

Parameter	Parameter Description	Stationary	Flaring
R	Source dimension (cm)	2×10^{16}	2×10^{16}
B	Magnetic field (G)	0.12	0.03
t_{esc}	Escape timescale (R/c)	6	1.5
ℓ_{inj}	Compactness injected as particle energy	6×10^{-5}	3×10^{-4}
s	Slope of the injected stationary power law	1.6	...
γ_{max}	Maximum Lorentz factor of the injected stationary power law	3×10^5	...
$\gamma_{\text{c,max}}$	Maximum Lorentz factor of Gaussian injection for the flaring component	...	7×10^5
δ	Beaming factor	18	18

that from the lower energy ones, as after the peak no further increase of the (LECS) flux is observed; this in particular requires that the injection stop after reaching the highest energies.

5. The total decay timescale might be dominated by the achromatic crossing-time effects, although the initial fading might be determined by different cooling timescales.

The acceleration term has then been described as a Gaussian distribution in energy, centered at a typical particle Lorentz factor $\gamma_c(t)$ and with width $\sigma = 0.01\gamma_c(t)$, exponentially evolving with time: $\gamma_c(t) \propto e^{-(t_{\max}-t)}$, where t_{\max} corresponds to the end of the acceleration phase, when the maximum $\gamma_{c,\max}$ is reached. The injected luminosity is assumed to be constant in time.

The duration of the injection, assumed to correspond to the light crossing time of the emitting region, is such that it mimics the passage of a shock front (i.e., a moving surface passing through the region in the same time interval; see Chiaberge & Ghisellini 1999).

It should also be noted that, within this scenario, the symmetry between the rise and decay in the soft energy light curve seems to suggest that if the energy where most of the power is released is determined by the balance between the acceleration and cooling rates, at this very same energy the latter timescales are comparable to the light crossing time of the region.

The predictions of the model are shown in Figures 6 and 7 in the form of light curves and spectra at different times, respectively. In particular, in Figure 6 the light curves (normalized over the stationary component) at the two centroid energies of the soft and hard bands considered in the data analysis are reported. The presence of a hard lag is clearly visible as well as the larger variability amplitude at higher frequencies. Also, the spectral evolution, reported in Figure 7 in νF_ν , in the observed energy range, seems to be at least in qualitative agreement with what was observed (compare with Fig. 3).

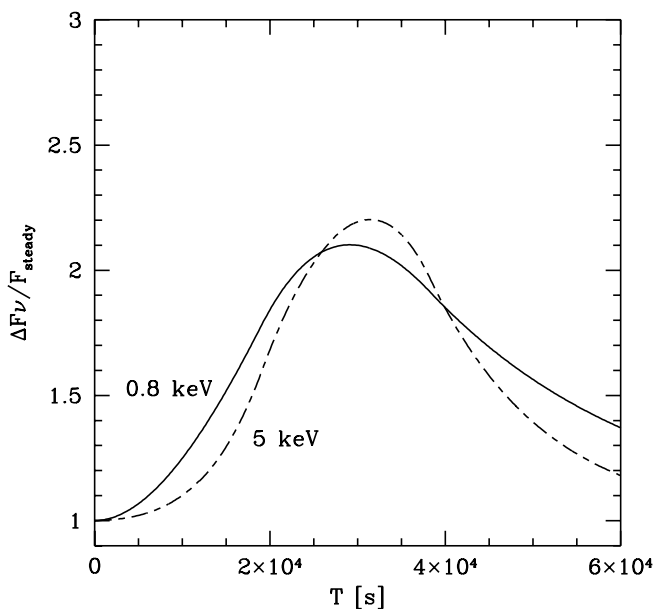


FIG. 6.—Light curves computed from the model, at the centroid energies of the soft and hard band considered in the data analysis. The vertical axis represents the variations normalized to the flux of the stationary component.

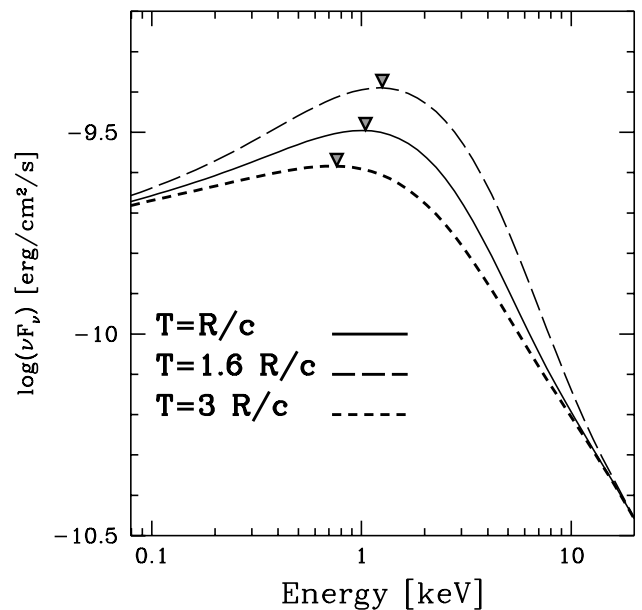


FIG. 7.—X-ray spectra at different times, as derived from the model. On each spectrum we marked the position of the synchrotron peak with a symbol.

A posteriori it is important to notice that the inclusion of a quasi-stationary component and of high-energy emission (from synchrotron self-Compton) are indeed crucial in order to reproduce the retarded spectral variability at energies above a few keV. This constitutes a further difference with respect to the discussion of Maraschi et al. (1999), where a simplified description of the time decay was used, based on evidence for an energy dependence of the flare decay timescale (obtained by modeling the decay with no baseline).

6. CONCLUSIONS

BeppoSAX has observed Mrk 421 in 1997 and 1998. We analyzed and interpreted the combined spectral and temporal evolution in the X-ray range. During these observations, the source has shown a large variety of behaviors, both concerning the X-ray band itself and its variability properties with respect to the γ -ray one, providing us with a great wealth of information but at the same time revealing a richer than expected phenomenology.

Several important results follow from this work.

1. The X-ray and 2 TeV light curves peak simultaneously *within one hour*, although the halving time in the TeV band seems shorter than those at LECS and MECS energies (see Maraschi et al. 1999).

2. The detailed comparison of 0.1–1.5 keV and 3.5–10 keV band light curves shows that the higher energy band lags the softer one, with a delay of the order of 2–3 ks. This finding is the opposite of what has been commonly observed in HBL X-ray spectra (see Paper I).

3. Moreover, extracting LECS+MECS spectra for $\lesssim 5$ ks intervals, we were able to follow in detail the spectral evolution during the flare. For the *first* time we could quantitatively track the shift of the peak of the synchrotron component moving to higher energy during the rising phase of the flare and then receding.

4. An energy dependence of the shape of the light curve during the flare has been revealed: at low energies, the

shape is consistent with being symmetric, while at higher energies it is clearly asymmetric (faster rise) (see Paper I).

5. Evidence has been found for the presence of the IC component and, more important, for its substantial variability, which is possibly delayed with respect to the synchrotron one.

These findings provide several temporal and spectral constraints on any model. In particular, they seem to reveal the first direct signature of the ongoing particle acceleration mechanism, progressively “pumping” electrons from lower to higher energies. The measure of the delay between the peaks of the light curves at the corresponding emitted frequencies thus provides a tight constraint on the timescale of the acceleration process.

Indeed, within a single emission-region scenario, we have been able to reproduce the sign and amount of lag by postulating that particle acceleration follows a simple exponential law in time, stops at the highest particle energies, and lasts for an interval comparable to the light crossing time of the emitting region. If this timescale is intrinsically linked to the typical source size, we indeed expect the observed light curve to be symmetric at the energies where the bulk of power is concentrated and an almost achromatic decay.

The same model can account for the spectral evolution (shift of the synchrotron peak) during the flare.

The other very important clue derived from the analysis is the presence of a quasi-stationary contribution to the emission, which seems to be dominated by a highly variable peaked spectrum, possibly maintaining a quasi-rigid shape during flares. The decomposition of the observed spectrum into these two components might allow us to determine the nature and modality of the energy dissipation in relativistic jets.

We are grateful to the *BeppoSAX* Science Data Center (SDC) for their invaluable work and for providing the standardized product data archive and to the *Rossi X-Ray Timing Explorer* ASM Team. We thank Gianpiero Tagliaferri and Paola Grandi for their contribution to our successful *BeppoSAX* program and for useful comments and the anonymous referee for suggestions that have improved the clarity of the paper. A. C., M. C., and Y. H. Z. acknowledge the Italian MURST for financial support. This research was supported in part by the National Science Foundation under Grant No. PHY94-07194 (AC). Finally, G. F. thanks Cecilia Clementi for providing tireless stimulus.

APPENDIX A

A CAVEAT ON CONTINUOUSLY CURVED SPECTRAL MODELS

The increasing quality of the available X-ray spectral data, both in terms of signal-to-noise ratio and energy resolution, has made it necessary to consider more complex fitting models. One of the most interesting continuum features in the X-ray spectra of blazars is the curvature of the synchrotron component as good quality data could enable us to estimate the energy of the emission peak. As clearly the traditional single or broken power-law models are unsatisfactory, we developed the curved spectral model presented in this paper: a simple analytic expression representing a continuous curvature, two “pivoting” points—useful for analysis purposes—asymptotically joining two power-law branches, the slope of which is completely determined by the behavior of the function at the pivoting energies.

Another increasingly popular model has been introduced by Giommi et al. (1998) (to reproduce *BeppoSAX* data of PKS 2155–304 and then used also for Mrk 421 by Guainazzi et al. 1999 and Malizia et al. 2000), but unfortunately this is affected by a problem that can lead to misleading results.

This more generally occurs for all curved continuum models defined as:

$$F(E) = E^{-\tilde{\alpha}(E)}, \quad (\text{A1})$$

where the function $\alpha(E)$ is suitably defined to smoothly change between two asymptotic values α_1 and α_2 . The specific choice by Giommi et al. (1998) is

$$\tilde{\alpha}(E) = f(E)\alpha_1 + [1 - f(E)]\alpha_2, \quad (\text{A2})$$

with

$$f(E) = (1 - e^{-E/E_0})^\beta. \quad (\text{A3})$$

Thus $\tilde{\alpha} \rightarrow \alpha_1$ for $E \ll E_0$, and $\tilde{\alpha} \rightarrow \alpha_2$ for $E \gg E_0$. While this is exactly the behavior of the spectral index function, this does not correspond to the real spectral index of the function $F(E)$, conventionally defined as

$$\alpha(E) \equiv -\frac{d \ln F(E)}{d \ln E}. \quad (\text{A4})$$

In fact, for $F(E) \equiv E^{-\tilde{\alpha}(E)}$, this yields

$$\alpha(E) = \tilde{\alpha}(E) + \ln E \frac{d\tilde{\alpha}(E)}{d \ln E} = \tilde{\alpha}(E) + \delta_{\tilde{\alpha}}(E), \quad (\text{A5})$$

thus including an unavoidable term $\delta_{\tilde{\alpha}}(E)$, which is present because of the not vanishing (by definition) derivative of $\tilde{\alpha}(E)$.

For the above specific choice of $\tilde{\alpha}(E)$:

$$\delta_{\tilde{\alpha}}(E) = \beta \frac{E}{E_0} \ln E (\alpha_1 - \alpha_2) e^{-E/E_0} (1 - e^{-E/E_0})^{\beta-1}. \quad (\text{A6})$$

The real spectral index then takes a value (sensibly) different from the one expected over a large range of energies.

The effect can be better illustrated with an example. Let us consider a set of spectral parameters that would well reproduce the spectrum of the peak of the 1998 flare of Mrk 421: $\alpha_1 = 0.75$, $\alpha_2 = 1.5$, $E_0 = 3.5$ keV, $\beta = 1.0$. In Figure 8, we show the spectrum together with $\tilde{\alpha}(E)$ and $\alpha(E)$ as derived by the model over an energy interval broader than that effectively covered by data. For reference, we also plotted the values of α derived from our curved model fits to show that the real spectral index $\alpha(E)$ matches them. A few features emerge.

1. According to $\tilde{\alpha}(E)$, between E_0 and 10 keV there is an apparent wiggle in the spectrum, which steepens beyond the supposedly asymptotic value α_2 before reaching it at about 30 keV.
2. Within the 0.1–10 keV range, $\alpha(E)$ and $\tilde{\alpha}(E)$ never match each other except for $E = 1$ keV, when $\delta_{\tilde{\alpha}}(E)$ vanishes.
3. The range spanned by the true spectral index is broader, and in particular it is always steeper than the value expected on the basis of $\tilde{\alpha}(E)$ in the whole band 1–20 keV. $\Delta\alpha$ can be as much as $+0.42$ (at $E \simeq 5.5$ keV).
4. At no energy in the 0.1–10 keV band does the actual spectrum have a slope equal to either α_1 or α_2 , and thus these two parameters do not have any real descriptive meaning (this is strikingly illustrated by the displacement of the real data points from the expected curve).
5. The total change of slope in the 0.1–10 keV interval would be expected to be $\Delta\tilde{\alpha} \simeq 0.68$ while it actually turns out to be 1.04 (and even more dramatically between 0.5 and 5.0 keV, $\Delta\tilde{\alpha} \simeq 0.46$ while for the data it is 0.86; see Table 1).

Summarizing, there is no way to define a curved continuum model by means of a suitable function describing the power-law exponent.

APPENDIX B

MORE DETAILS ON THE ADOPTED CURVED MODEL

The relationship between $\alpha(E)$ and $\alpha_{-\infty}$ and $\alpha_{+\infty}$ is

$$\alpha(E) \equiv -\frac{d \ln F(E)}{d \ln(E)} = \alpha_{-\infty} - (\alpha_{-\infty} - \alpha_{+\infty}) \frac{(E/E_B)^f}{1 + (E/E_B)^f}, \quad (\text{B1})$$

yielding

$$\alpha_{-\infty} = \frac{B(1+A)\alpha_1 - A(1+B)\alpha_2}{B-A} \quad (\text{B2})$$

$$\alpha_{+\infty} = \frac{(1+B)\alpha_2 - (1+A)\alpha_1}{B-A}, \quad (\text{B3})$$

where $A = (E_1/E_B)^f$, and $B = (E_2/E_B)^f$.

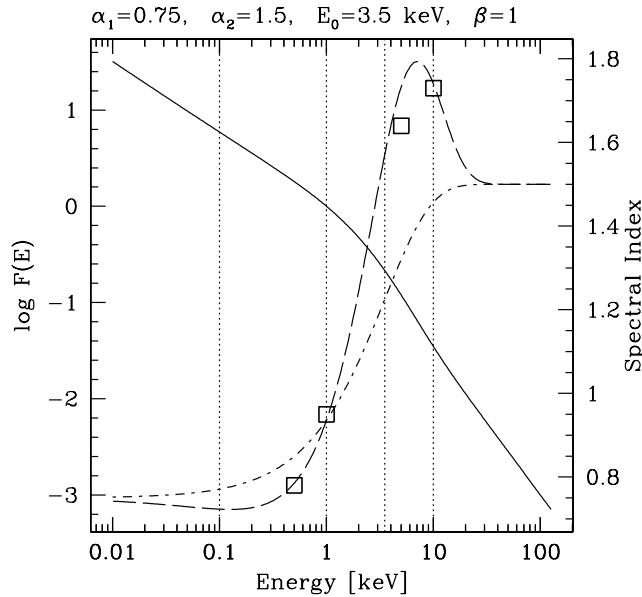


FIG. 8.—Example of the fitting spectral model used by Giommi et al. (1998), for a choice of model parameters suited to reproduce the spectral properties of the 1998 flare (shown on top of the figure box). The solid line is the spectrum (scale on the left y-axis). The dot-dashed line is the predicted spectral index $\tilde{\alpha}(E)$, and the dashed line is the “true” spectral index of the resulting $F(E)$ (both with the scale on the right y-axis). The squares represent the values of the spectral index at the same energies reported in Table 1. Vertical bars indicate a few relevant reference energies, namely 0.1 and 10 keV, that are the limits of the band covered by LECS and MECS, 1 keV as the energy at which the model is normalized to unity, and E_0 .

TABLE 6
LECS AND MECS BROKEN POWER-LAW MODEL SPECTRAL FIT: 1997 AND 1998

ORBITS	GALACTIC ABSORBING COLUMN ^a				FREE ABSORBING COLUMN ^b				
	α_1	α_2	E_{break} (keV)	χ^2_{ν}	N_{H} (10^{20} cm^{-2})	α_1	α_2	E_{break} (keV)	χ^2_{ν}
1997 April 29 to May 5									
1-3	0.96 ^{+0.05} _{-0.07}	1.71 ^{+0.04} _{-0.03}	1.37 ^{+0.18} _{-0.19}	1.71	2.50 ^{+0.32} _{-0.30}	1.26 ^{+0.08} _{-0.08}	1.77 ^{+0.06} _{-0.05}	2.25 ^{+0.23} _{-0.23}	1.37
4-7	1.01 ^{+0.04} _{-0.04}	1.79 ^{+0.03} _{-0.03}	1.23 ^{+0.12} _{-0.10}	1.55	1.96 ^{+0.37} _{-0.41}	1.14 ^{+0.13} _{-0.17}	1.80 ^{+0.04} _{-0.07}	1.38 ^{+0.27} _{-0.22}	1.51
8-10	0.93 ^{+0.07} _{-0.09}	1.77 ^{+0.04} _{-0.04}	1.19 ^{+0.17} _{-0.15}	1.38	2.92 ^{+0.43} _{-0.43}	1.40 ^{+0.10} _{-0.10}	1.95 ^{+0.13} _{-0.11}	2.90 ^{+0.48} _{-0.51}	1.23
11-12	1.04 ^{+0.05} _{-0.05}	1.77 ^{+0.04} _{-0.04}	1.41 ^{+0.18} _{-0.16}	1.26	1.97 ^{+0.45} _{-0.43}	1.16 ^{+0.14} _{-0.16}	1.77 ^{+0.05} _{-0.05}	1.53 ^{+0.44} _{-0.24}	1.22
13-15	0.97 ^{+0.04} _{-0.05}	1.82 ^{+0.03} _{-0.03}	1.26 ^{+0.11} _{-0.10}	1.24	1.94 ^{+0.43} _{-0.43}	1.09 ^{+0.15} _{-0.17}	1.82 ^{+0.04} _{-0.04}	1.35 ^{+0.24} _{-0.17}	1.21
16-18	1.00 ^{+0.07} _{-0.08}	1.76 ^{+0.05} _{-0.05}	1.14 ^{+0.17} _{-0.13}	1.10	1.62 ^{+0.68} _{-0.33}	1.01 ^{+0.25} _{-0.25}	1.76 ^{+0.05} _{-0.05}	1.14 ^{+0.31} _{-0.15}	1.12
19-20	0.97 ^{+0.05} _{-0.06}	1.68 ^{+0.04} _{-0.04}	1.15 ^{+0.12} _{-0.10}	1.41	1.58 ^{+0.49} _{-0.46}	0.96 ^{+0.18} _{-0.20}	1.68 ^{+0.04} _{-0.04}	1.14 ^{+0.17} _{-0.13}	1.44
21-23	0.94 ^{+0.04} _{-0.04}	1.73 ^{+0.03} _{-0.03}	1.28 ^{+0.09} _{-0.08}	1.84	1.89 ^{+0.34} _{-0.33}	1.04 ^{+0.12} _{-0.12}	1.73 ^{+0.03} _{-0.03}	1.34 ^{+0.16} _{-0.12}	1.81
24-25	0.95 ^{+0.06} _{-0.07}	1.70 ^{+0.04} _{-0.04}	1.31 ^{+0.17} _{-0.16}	1.13	2.41 ^{+0.34} _{-0.33}	1.25 ^{+0.08} _{-0.08}	1.77 ^{+0.07} _{-0.06}	2.31 ^{+0.31} _{-0.28}	0.98
26-27	0.97 ^{+0.06} _{-0.06}	1.76 ^{+0.04} _{-0.03}	1.28 ^{+0.17} _{-0.18}	1.14	2.32 ^{+0.32} _{-0.33}	1.27 ^{+0.07} _{-0.09}	1.80 ^{+0.08} _{-0.07}	2.30 ^{+0.31} _{-0.28}	0.99
28-30	1.09 ^{+0.06} _{-0.07}	1.77 ^{+0.04} _{-0.04}	1.33 ^{+0.26} _{-0.16}	1.24	2.06 ^{+0.50} _{-0.57}	1.25 ^{+0.18} _{-0.22}	1.77 ^{+0.05} _{-0.05}	1.54 ^{+0.92} _{-0.35}	1.21
31-32	1.18 ^{+0.04} _{-0.05}	2.04 ^{+0.09} _{-0.09}	2.34 ^{+0.19} _{-0.27}	0.94	2.20 ^{+0.45} _{-0.43}	1.32 ^{+0.11} _{-0.11}	2.06 ^{+0.11} _{-0.10}	2.43 ^{+0.25} _{-0.28}	0.80
33-34	1.08 ^{+0.09} _{-0.10}	2.01 ^{+0.08} _{-0.08}	1.14 ^{+0.16} _{-0.13}	1.36	3.08 ^{+0.55} _{-0.53}	1.64 ^{+0.13} _{-0.13}	2.28 ^{+0.27} _{-0.21}	3.12 ^{+0.61} _{-0.80}	1.30
35-37	1.22 ^{+0.06} _{-0.07}	1.99 ^{+0.05} _{-0.05}	1.23 ^{+0.17} _{-0.15}	1.20	2.56 ^{+0.38} _{-0.38}	1.58 ^{+0.10} _{-0.10}	2.15 ^{+0.13} _{-0.12}	2.64 ^{+0.39} _{-0.50}	1.06
38-40	1.07 ^{+0.06} _{-0.07}	1.90 ^{+0.05} _{-0.05}	1.11 ^{+0.11} _{-0.11}	1.34	2.82 ^{+0.34} _{-0.37}	1.55 ^{+0.08} _{-0.10}	2.06 ^{+0.12} _{-0.14}	2.83 ^{+0.39} _{-0.68}	1.15
41-42	1.11 ^{+0.07} _{-0.08}	1.85 ^{+0.06} _{-0.06}	1.25 ^{+0.22} _{-0.19}	0.74	1.71 ^{+0.62} _{-0.61}	1.14 ^{+0.22} _{-0.27}	1.85 ^{+0.07} _{-0.06}	1.28 ^{+0.39} _{-0.26}	0.75
1998 April 21									
1-2	0.86 ^{+0.06} _{-0.06}	1.57 ^{+0.05} _{-0.05}	1.23 ^{+0.14} _{-0.12}	0.99	2.01 ^{+0.66} _{-0.49}	0.99 ^{+0.24} _{-0.18}	1.57 ^{+0.06} _{-0.05}	1.32 ^{+0.94} _{-0.19}	0.96
3	0.91 ^{+0.05} _{-0.06}	1.55 ^{+0.05} _{-0.05}	1.53 ^{+0.22} _{-0.23}	1.07	1.71 ^{+0.53} _{-0.54}	0.94 ^{+0.17} _{-0.22}	1.55 ^{+0.06} _{-0.06}	1.56 ^{+0.66} _{-0.36}	1.08
4	0.84 ^{+0.05} _{-0.04}	1.52 ^{+0.04} _{-0.04}	1.56 ^{+0.27} _{-0.17}	1.43	2.20 ^{+0.27} _{-0.28}	1.03 ^{+0.07} _{-0.08}	1.56 ^{+0.06} _{-0.06}	2.13 ^{+0.32} _{-0.36}	1.15
5	0.84 ^{+0.04} _{-0.04}	1.47 ^{+0.04} _{-0.04}	1.39 ^{+0.16} _{-0.12}	1.35	2.29 ^{+0.25} _{-0.25}	1.08 ^{+0.06} _{-0.06}	1.56 ^{+0.08} _{-0.12}	2.47 ^{+0.39} _{-0.97}	1.32
6	0.82 ^{+0.05} _{-0.06}	1.42 ^{+0.04} _{-0.04}	1.21 ^{+0.21} _{-0.15}	1.55	2.34 ^{+0.28} _{-0.29}	1.10 ^{+0.07} _{-0.09}	1.47 ^{+0.06} _{-0.05}	2.01 ^{+0.42} _{-0.42}	1.28
7	0.82 ^{+0.05} _{-0.05}	1.45 ^{+0.04} _{-0.04}	1.28 ^{+0.15} _{-0.12}	1.05	2.02 ^{+0.41} _{-0.43}	0.97 ^{+0.13} _{-0.16}	1.46 ^{+0.05} _{-0.05}	1.46 ^{+0.46} _{-0.26}	1.00
8-9	0.88 ^{+0.03} _{-0.04}	1.44 ^{+0.03} _{-0.03}	1.27 ^{+0.11} _{-0.11}	1.71	2.00 ^{+0.34} _{-0.27}	1.01 ^{+0.13} _{-0.10}	1.44 ^{+0.04} _{-0.04}	1.41 ^{+0.75} _{-0.17}	1.57
10-12	0.90 ^{+0.03} _{-0.03}	1.47 ^{+0.03} _{-0.03}	1.34 ^{+0.10} _{-0.09}	0.96	1.80 ^{+0.24} _{-0.25}	0.96 ^{+0.08} _{-0.09}	1.47 ^{+0.03} _{-0.03}	1.41 ^{+0.18} _{-0.14}	0.93
13-16	0.95 ^{+0.03} _{-0.03}	1.52 ^{+0.03} _{-0.03}	1.46 ^{+0.16} _{-0.14}	1.38	2.25 ^{+0.21} _{-0.20}	1.16 ^{+0.05} _{-0.05}	1.58 ^{+0.06} _{-0.06}	2.35 ^{+0.27} _{-0.34}	1.01
1998 April 23									
1-5	0.96 ^{+0.03} _{-0.03}	1.58 ^{+0.03} _{-0.03}	1.40 ^{+0.12} _{-0.10}	1.76	2.09 ^{+0.32} _{-0.25}	1.13 ^{+0.10} _{-0.09}	1.59 ^{+0.07} _{-0.03}	1.70 ^{+0.67} _{-0.25}	1.50
6-11	0.98 ^{+0.02} _{-0.02}	1.67 ^{+0.02} _{-0.02}	1.30 ^{+0.07} _{-0.07}	2.45	1.92 ^{+0.21} _{-0.21}	1.09 ^{+0.08} _{-0.08}	1.68 ^{+0.03} _{-0.03}	1.43 ^{+0.19} _{-0.13}	2.31
12-19	1.07 ^{+0.02} _{-0.02}	1.69 ^{+0.03} _{-0.03}	1.46 ^{+0.09} _{-0.09}	1.79	2.02 ^{+0.18} _{-0.18}	1.20 ^{+0.06} _{-0.06}	1.69 ^{+0.03} _{-0.03}	1.62 ^{+0.19} _{-0.14}	1.37

^a Galactic hydrogen equivalent absorbing column is $N_{\text{H}}=(1.61 \pm 0.1) \times 10^{20} \text{ cm}^{-2}$ (Lockman & Savage 1995). The quoted errors are for 1σ for three parameters (i.e., $\Delta\chi^2 = 3.53$). The dof is 57.

^b Quoted errors are for 1σ for four parameters (i.e., $\Delta\chi^2 = 4.72$). The dof is 56.

APPENDIX C

MORE DETAILS ON THE BROKEN POWER-LAW FITS

Table 6 reports the best-fit values for the relevant parameters for the broken power-law model.

REFERENCES

- Boella, G., Butler, R. C., Perola, G. C., Piro, L., Scarsi, L., & Bleeker, J. A. M. 1997, *A&AS*, 122, 299
 Canizares, C., & Kruper, J. 1984, *ApJ*, 278, L99
 Catanese, M., & Sambruna, R. M. 2000, *ApJ*, 534, L39
 Chiaberge, M., & Ghisellini, G. 1999, *MNRAS*, 306, 551
 Chiappetti, L., & Dal Fiume, D. 1997, in Proc. of the 5th Workshop, Data Analysis in Astronomy, ed. V. Di Gesù et al. (Singapore: World Scientific), 101
 Chiappetti, L., et al. 1999, *ApJ*, 521, 552
 Fiore, F., Guainazzi, M., & Grandi, P. 1999, Cookbook for *BeppoSAX* NFI Spectral Analysis (Roma, Italy: SDC)
 Fossati, G., & Haardt, F. 1997, Scientific Report on Low Energy Absorption Features Detected by *BeppoSAX* LECS in Bright Blazar Targets. Rept. no. Ref. SISSA 146/97/A; preprint (astro-ph/9804282)
 Fossati, G., Maraschi, L., Celotti, A., Comastri, A., & Ghisellini, G. 1998a, *MNRAS*, 299, 433
 Fossati, G., et al. 1998b, *Nucl. Phys. B Supp.*, 69, 423
 ———. 2000, *ApJ*, 541, (Paper I)
 Georgopoulos, M., & Marscher, A. P. 1998, *ApJ*, 506, L11
 Ghisellini, G., & Madau, P. 1996, *MNRAS*, 280, 67
 Ghisellini, G., Celotti, A., Fossati, G., Maraschi, L., & Comastri, A. 1998, *MNRAS*, 301, 451
 Giommi, P., et al. 1998, *A&A*, 333, L5
 ———. 1999, *A&A*, 351, 59
 Guainazzi, M., et al. 1999, *A&A*, 342, 124
 Inoue, S., & Takahara, F. 1996, *ApJ*, 463, 555
 Kirk, J. G., Rieger, F. M., & Mastichiadis, A. 1998, *A&A*, 333, 452
 Krawczynski, H., Coppi, P. S., Maccarone, T., & Aharonian, F. A. 2000, *A&A*, 353, 97
 Lockman, F. J., & Savage, B. D. 1995, *ApJS*, 97, 1
 Macomb, D. J., et al. 1995, *ApJ*, 449, L99 (erratum 459, L111 [1996])
 Malizia, A., et al. 2000, *MNRAS*, 312, 123
 Maraschi, L., et al. 1999, *ApJ*, 526, L81
 Padovani, P., & Giommi, P. 1995, *ApJ*, 444, 567
 Pian, E., et al. 1998, *ApJ*, 492, L17
 ———. 1999, *ApJ*, 521, 112

- Sambruna, R. M., George, I. M., Madejski, G., Urry, C. M., Turner, T. J., Weaver, K. A., Maraschi, L., & Treves, A. 1997, *ApJ*, 483, 774
- Sambruna, R. M., Ghisellini, G., Hooper, E., Kollgaard, R. I., Pesce, J. E., & Urry, C. M. 1999, *ApJ*, 515, 140
- Sambruna, R. M., & Mushotzky, R. F. 1998, *ApJ*, 502, 630
- Sembay, S., Warwick, R. S., Urry, C. M., Sokoloski, J., George, I. M., Makino, F., Ohashi, T., & Tashiro, M. 1993, *ApJ*, 404, 112
- Sikora, M., Begelman, M. C., & Rees, M. J. 1994, *ApJ*, 421, 153
- Tagliaferri, G., et al. 2000, *A&A*, 354, 431
- Takahashi, T., et al. 1996, *ApJ*, 470, L89
- Tavecchio, F., Maraschi, L., & Ghisellini, G. 1998, *ApJ*, 509, 608
- Urry, C. M., & Padovani, P. 1995, *PASP*, 107, 803
- Zhang, Y. H., et al. 1999, *ApJ*, 527, 719